Received: 05 August 2024 | Revised: 22 September 2024 | Accepted: 07 October 2024

https://doi.org/10.56946/jce.v3i2.449

Journal of Chemistry and Environment

Research Article

Biosynthesis, Characterization, Antibacterial Activities, and Photocatalysis of Zinc Oxide Nanoparticles Using *Allium Ambelloprasum (leeks)* Leaves Extract

Nabil Abduraqeb Alhemiary[1,2*], Yasser Saaed Ibrahem[3]

[1]Department of Chemistry, College of Science and Arts- Sharourah, Najran University, Sharourah, Saudi Arabia.
[2]Department of Chemistry, College of Science, Ibb University, P. O. Box 70270, Ibb, Yemen.
[3]Department of Biology, College of Science, Cairo university, Cairo, Egypt.
*Correspondence: dralhemiary@gmail.com

Abstract

The biosynthesis of nanomaterials using phytochemicals found in plants has attracted a lot of interest and is gaining traction as a viable alternative to traditional chemical processes. In the current work, we used the aqueous leaf extract of *Allium ampeloprasum (leek)* as a reducing and stabilizing agent for the simple bio-fabrication of zinc oxide (ZnO) nanoparticles (NPs), owing to its alkaloids, coumarins, and flavonoids. Several methods, including, XRD, SEM, EDX, FT-IR, TEM, UV-visible spectroscopy, and TGA, were used to analyze the characteristics of the bio-fabricated ZnO-NPs. An XRD study revealed that ZnO-NPs had a monoclinic structure with a crystallite dimension of 25.75 nm. The spherical structure of ZnO-NPs is confirmed by TEM and SEM morphological pictures, and their dispersion across surfaces shows decreased agglomerations. ZnO-NPs had a significant optical absorbance in the UV area at 368 nm and a large bandgap, indicating surface oxygen vacancies and charge carriers. The existence of Zn and O elements, as well as their Zn bonds, was identified using EDX and FT-IR spectroscopy. The photodegradation of methylene blue (MB) dye was studied using UV light irradiation, with a maximum degradation efficiency of 90.13% attained after 120 minutes of irradiation. Gram-positive Gram-negative bacteria and *E. coli* ZnO-NPs were tested against *S.ococcus* aureus, which showed the maximum zone inhibition (15.01 ± 0.85 mm) compared to *E. coli* (13.34 ± 0.04 mm). Thus, the degradation efficiency for MB dye and the zone inhibition results for both Gram-positive and Gram-negative bacteria indicate that the bio-fabricated ZnO-NPs from *A. ampeloprasum (leek*) leaves may have biological and environmental uses.

Keywords: Biosynthesis, *allium ampeloprasum* (leek), ZnO-NPs, photodegradation, antibacterial.

1. Introduction

Alot of research has been done on metal-based nanoparticles due to their special characteristics, such as copper, silver, gold, titanium, zinc oxide, titanium oxide, and copper oxide [1]. Various methods, such as chemical and physical reduction and microwave-aided, can be used to create these nanoparticles. However, there are several problems associated with these processes by the implementation in the biological environment because of the use of toxic materials as reducing agents [2]. Green nanotechnology is an ideal way to lessen the harmful impacts of producing and using nanoparticles, thereby reducing the risk associated with the nanotechnology [3]. Green nanotechnology is concerned with production of nanomaterials and their uses in the food, energy, medicinal, sensor, and optoelectronics sectors [4]. Metal nanoparticles (NPs) and metal

oxide nanostructures can be generated via a variety of chemical and physical techniques, including sputtering, lithography, and electrospinning. Nevertheless, they come at a high cost, and working with hazardous substances puts your health in danger. In this sense, no dangerous chemicals, high-pressure reactors, or high temperatures are needed for the green synthesis method. The main benefit is that it produces biodegradable trash with a lower chance of contamination in the end [3].

Zinc oxide nanoparticles (ZnO-NPs) are the most widely used metal oxide nanoparticles due to their easily modifiable wide bandgap of 3.37 eV, and high excitation binding energy of 60 meV. This allows ZnO-NPs effectively imitate a strong photocatalytic and photo oxidizing moiety that targets both biological and chemical species [5]. Zinc is a trace element that is less toxic to the body, and the dissolved Zn^{+2} of zinc oxide is biocompatible with the physiological system[6]. The biodegradability of ZnO-based materials has been demonstrated in both bulk phases and as nanoparticles. Additionally, by damaging the cell membranes of intracellular bacteria, zinc ions serve as the main mediators of their toxicity [7]. A variety of plants have been extracted to create ZnO-NPs through green synthesis, such as Garlic (*A. sativum*) [8], Cardamom [9], *C. fistula* and *M. azadarch* [3], *A. vera* (coffee) [10], Z. *officinale* (ginger) [11], *O. peel* [12], and *L. adenosis* (koseret) [13].

Allium ampeloprasum (leek) is a hardy biennial that does not grow a hard bulb like onions or garlic [14]. One of Europe's most important veggies to cultivate, from the Balkan Peninsula to Ireland, as well as in western Asia, is *A. ampeloprasum*. (e.g., Middle East) [15]. *A. ampeloprasum* has a large amount of organosulfur compounds, with gamma-glutamyl peptides prevailing over alliin and allicin. Apart from the presence of saponins, this imparts to the leeks a sweet onion flavor and a moderate pungent aroma, as opposed to the powerful pungent perfume of onion and garlic [16]. The green leaves and white shafts or bulbs of *A. ampeloprasum* are rich stores of secondary metabolites, including flavonoids, phenolic acids, polyphenols, and saponins [14]. *A. ampeloprasum* bulbs exhibited more phenol content and antioxidant activity than typical garlic bulbs, according to reported research [17]. Apart from its culinary uses, a number of studies have documented the medical applications of *A. ampeloprasum*, including anti-proliferative [18], anti-bacterial [19], anti-fungal[20], antiulcer effects [16], , anticancer [15], anti-inflammatory [16], and anti-oxidative[16]. Furthermore, in a rat model of diabetes produced by alloxan, it demonstrated hypoglycemic, hypolipidemic, and anti-oxidative properties[21]. This strategy has advantages: the precursor is less expensive, and the product is purer and comes in larger quantities. Additional advantages include its speed and environmentally friendly methodology. It does not the use of any intermediate compounds or costly equipment. Considering nutritional values Few characterizations of new metabolites in *A. ampeloprasum*, commonly known as leeks, have been conducted thus far, and this food plant has not received much attention in terms of its therapeutic potential. For this reason, the present work offers a biosynthesis of zinc oxide nanoparticles (ZnO-NPs) using A. ampeloprasum leaves that contain a variety of phytochemicals to produce an aqueous extract that is then used to produce and stabilize ZnO-NPs. This process has two advantages: the precursor is less expensive, and the product is purer and comes in larger quantities. Additional advantages include its speed and environmentally friendly methodology. It does not necessitate the use of any intermediate compounds or costly equipment. Bio-fabricated ZnO-NPs were successfully characterized by FTIR, XRD, UV spectroscopy, SEM, TEM, TGA, and EDX techniques Additionally, the mechanism of MB dye degradation under UV light was explored using bio-fabricated ZnO-NPs with photocatalytic properties. The biosynthesized NPs' antibacterial activity was investigated and evaluated against two harmful bacteria.: gram-positive S. aureus and gram-negative E. coli.

2. Materials and Methods

2.1. Chemicals and materials

The following chemicals The following chemicals, ethanol, sodium hydroxide (NaOH), and zinc acetate ($Zn(CH_3COO)_2{\cdot}2H_2O$) were acquired from Sigma Aldrich (Taufkirchen, Germany) . During the trials, deionized water that had undergone double distillation was utilized. The pH values

were controlled with sodium hydroxide. None of the analytical-grade compounds used in the tests require further purification.

2.2. Preparation of *A. ampeloprasum (leek)* leaves extract

The leaves of the locally grown *A. ampeloprasum* (leek) plant were obtained at localy market in Sharourah - Saudi Arabia. The leaves were repeatedly washed with tap water and then double-distilled water to remove the dust particles. The leaves were chopped into little bits and allowed to dry in the shade for 15 days. The dried leaves were pulverized into a powder. Subsequently, 10 g of the powder was mixed with 100 mL of double-distilled water in a reflux condenser for 45 minutes at 60 C^o. The green color of the distilled water shows that leaves were extracted [22]. After 45 minutes, the extract was allowed to cool to room temperature. Following that, the mixture was immediately used for the ZnO-NPs synthesis after being filtered via Whatman's No. 1 (11µm) filter paper.

2.3. Preparation of ZnO-NPs

Mix 4 grams of zinc acetate dehydrates with 100 milliliters of deionized water and magnetically stir for one hour at room temperature. The obtained *A. ampeloprasum* extract (20 ml) was then added to the zinc-based salt solution as indicated in Figure 1. The aforementioned combination's pH may be maintained up to 12 [23] by adding 1 M of NaOH solution dropwise at stirring constantly for two hours at 50°C and 400 rpm. This process was completed when dark yellow precipitates formed, indicating the creation of ZnO-NPs [24]. Precipitates were then separated using a centrifuge at 5,000 rpm for 20 minutes. After that, ethanol and deionized water were used three or four additional times for further purification. The precipitates were dried in an oven at 100°C, according to Figure 1. Following the drying process, the samples were calcined for two hours at 450°C in a muffle furnace, and the powders were then gathered for testing [11]. ZnO-NPs where ground until a fine powder was produced.

2.4. Characterization of ZnO-NPs

The bio-fabricated ZnO-NPs were characterized using a variety of methods, such as surface, optical, and structural morphology. The absorbance of the ZnO-NPs was measured using UV-Vis spectroscopy (Thermos Scientific 600 UV-Vis spectrophotometer, Waltham, MA, USA) in the 200–800 nm wavelength range. The surface chemistry of ZnO-NPs and the function of functional groups in phytochemicals in the bio-reduction were investigated using a Bruker FTIR spectrophotometer. The range in which the FTIR study was carried out was 4000–400 cm^{-1}. ZnO-NPs were analyzed using energy-dispersive X-ray (EDX) to ascertain their elemental configuration. However, ZnO-NPs form and size were ascertained using TEM. To get ready for TEM examination, the bio-fabricated ZnO nanoparticles underwent many washes in deionized water. Samples were placed on a carbon-coated copper grid, which was then taken off and given time to dry before analysis. Particle size distribution, morphology, and size were all determined by TEM analysis using a TEM (JEOL, JEM1011, Tokyo, Japan). At 100 Kv voltage, this microscope provided high-resolution two-dimensional images. Zeta potential analysis was utilized to determine the hydrodynamic particle size and net charge of ZnO nanoparticles, while XRD analysis was employed to identify the crystalline features of the produced nanomaterials [25]. An X-ray monochromator with a graphite unit that produced Cu-K radiation was used to conduct the X-ray particle diffraction (XRD) analysis (Shimadzu, Columbia, USA). Using the Brun Auer-Emmett-Teller (BET) method and Quanta Chrome Pore Size and Surface Area Analysis (Nova 3200e), the bio-fabricated Zn-ONPs were determined to evaluate their pore size distribution, surface area and pore volume.

2.5. Photodegradation of methylene blue

The efficiency of photocatalytic dye degradation of synthetic nanoparticles exposed to visible light was evaluated using MB (methylene blue) dye. Primarily, 10 mg of the produced nanoparticles were well disseminated in a 10 ppm MB solution utilizing the ultrasonication technique. The ultrasonicated solution was kept in a dark chamber and stirred with a magnetic stirrer for thirty minutes. Subsequently, UV light was applied to the samples. The samples were 8 cm apart, and the UV light source was an Xe lamp (λ = 400 nm). The samples that had been exposed to radiation were taken out at regular intervals and centrifuged at 1000 rpm to remove the nanoparticles. The dye solutions that had been collected were then measured using a

UV-visible spectrophotometer. The amount of MB dye that had broken down were measured at 665 nm absorbance. Quenching measurements, which may be used to find holes, superoxides, and free radicals, were utilized to study the active species of the photocatalyst. The efficiency of dye degradation with nanoparticles was calculated using formula (1) [26].

$$\text{MB dye degradation efficiency (\%)} = \frac{C_o - C}{C_o} \text{ x } 100 \quad (1)$$

Where C0 represents the MB dye solution's starting concentration (in milligrams per liter) and C represents the solution's concentration (in milligrams per liter) following a certain amount of radiation. Formula 2 was used to determine the half-life of MB dye degradation by biosynthesized NPs [26]:

$$\text{The half} - \text{life dye degradation} = [1 - \frac{C}{C_0}] \text{x} 100 \quad (2)$$

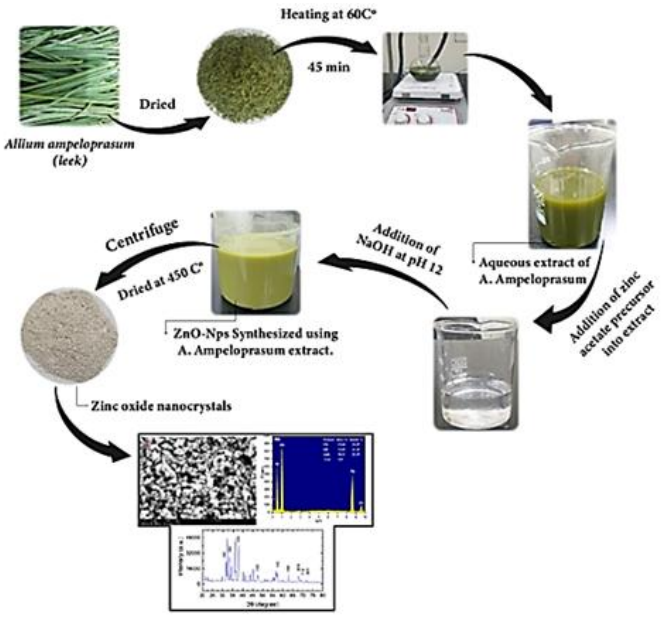

Figure 1. Diagram showing the steps involved synthesis of ZnO-AgNPs.

2.6. Antibacterial activities

The disc diffusion technique was used to assess the antibacterial activity of the nanoparticles against E. coli (ATCC 9637) and S. aureus (ATTC-6638). Nutritional agar was used for the solidification process, and it was put on sterile Petri dishes. A new culture of bacteria was put out over the hardened plates. Six-millimeter paper discs were filled with nanoparticles at four different doses (10, 20, 50, and 100 µg/ml). For 24 hours, the plates containing nanoparticles were incubated at 37 °C. In the end, the incubated plates developed inside the zones of inhibition. Standard amikacin discs were used to compare the measured bacterial activity. The inhibited region was measured on a millimeter scale. The synthesized nanoparticles' bacterial inactivity is demonstrated by the zone of inhibition[27].

3. Results and discussion

3.1. UV-vis spectral study of bio-fabricated ZnO-NPs.

The as-synthesised ZnO-NPs were stabilized by bioactive components found in the aqueous leaf extract of *A. ampeloprasum,* as demonstrated by the high absorption peak seen in the UV-visible spectroscopy. The details of the inquiry into ZnO-NPs' absorbance and bandgap band gap are shown in Figure 2a.

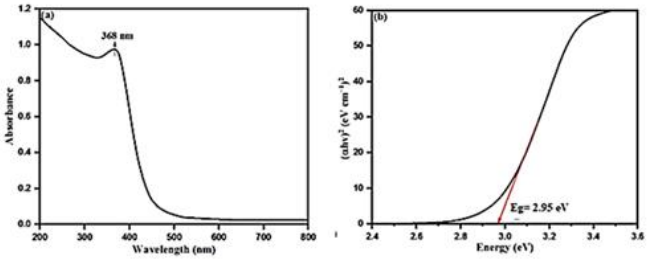

Figure 2. Diffuse reflectance spectrum observable in UV light (a), and bandgap characterization of bio-fabricated ZnO-NPs using a Tauc plot (b).

The bio-fabricated ZnO exhibited a characteristic absorption peak at 368 nm due to the valence band electrons switching across to the conduction band. In addition, the energy band gap was calculated using the following equation (3) using a Tauc plot [28].

$$(\alpha h\nu)^2 = [A(h\nu - E_g]^{\frac{1}{n}} \quad (3)$$

where 'Eg' is the energy bandgap, 'A' is the constant, 'h' is the Planks constant, and 'hν' is the energy of the incident photon. Plotting $(\alpha h\nu)^2$ against photon energy hν yielded the energy band (E_g) for ZnO, as Figure. 2b illustrates. The bandgap for ZnO-NPs 2.95 eV was obtained by using the Tauc Plot equation [29].

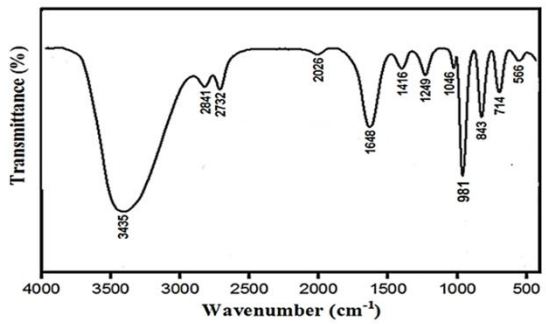

Figure 3. FT-IR spectrum for ZnO-NPs using an extract of *A. ampeloprasu.*

3.2. FT-IR spectra analysis of ZnO-NPs

FT-IR analysis was utilized to identify the primary functional groups responsible for the bio-formulated ZnO-NPs' reduction, stability, and capping[30]. Different absorption peaks were found at 3435, 1648, 1416, 1251, 1046, and 566 cm^{-1} in the FTIR spectrum (Figure 3). The robust peak seen at 3435 cm^{-1} may be attributed to the hydroxyl functional groups that are connected with the polyphenolic components of the extract of *A. ampeloprasum*, which helps stabilize by caping ZnO-NPs [31]. It was found that the vibrations of molecules of double-bonding carbon stretching were responsible for the additional absorption peaks seen at 1648 cm^{-1} and 1416 cm^{-1} [32]. However, a small band in the spectra at 1251cm^{-1} was identified as the C–N stretching of amines, along with other distinctive peaks at 891 cm^{-1} (-N–H, 1^{o}, and 2^{o} amine). They were capping agents on ZnO-NPs' surfaces. It was reported that alcohols from C to C, possibly capping the surface of ZnO-NPs, were the source of the band at 1046 cm^{-1} [33]. The production of ZnO-NPs by bioformulation was indicated by the observation of a broad absorption band at 566 cm^{-1}, which is characteristic of the Zn–O metal oxide bond[34]. The functional groups of biogenic ZnO-NPs that have been identified, such as amines, alcohols, carboxylic acids, phenols, and alkenes, significantly contributed to the stability; and capping of the bio-fabricated nanomaterials [35].

3.3. XRD analysis of ZnO-NPs.

ZnO-NPs that were bio-fabricated had their crystalline structure examined using XRD spectra. The bio-fabricated ZnO-NPs' XRD pattern is depicted in Figure 4, which is supported by the orientation plane-based peaks obtained at (100), (101), (102), (200), (110), (103), (200), (112), and (201). The corresponding values of 2θ are as follows: 31.912^{o}, 34.561^{o}, 36.538^{o}, 47.612^{o}, 6.752^{o}, 62.814^{o}, 68.011^{o}, 69.021^{o}, and 72.419^{o}. The bio-fabricated ZnO-NPs' polycrystalline structure was shown by the acquired XRD pattern, it is a result of the bio-fabricated ZnO-NPs hexagonal wurtzite structure. Based on the Powder Diffraction Joint Committee. (JCPD) criteria, these peaks are in good coordination with quartzite ZnO (card number 36–1451) [36]. In addition, these results are consistent with the results of Ali and co-workers for both pure ZnO-NPs and different ZnO-NPs concentrations[36]. Our study revealed that orientation peak (202) at 2θ = 72.691◦ had a strong intensity peak. This peak was ascribed to unreacted impurities in ZnO-NPs. The average size of ZnO-NPs is determined using Scherrer's formula, D = 0.94λ/β cos θ, where "λ" is the wavelength of the X-ray (1.54068^{-}).

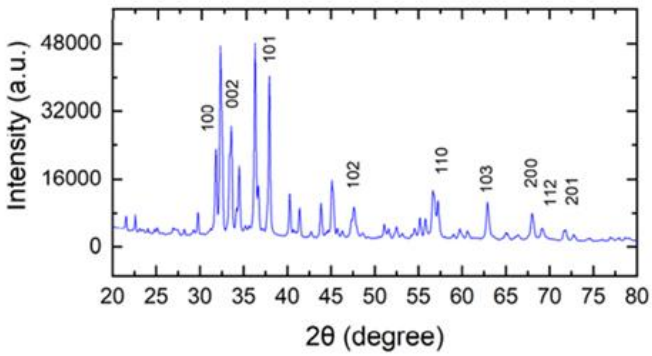

Figure 4. XRD spectra for the bio-fabricated ZnO-NPs.

The most intense diffraction peak's full width at half the maximum (FWHM) is denoted by β, which is detected to be 0.6912, and θ is diffraction angle (36.538◦) [36]. It was found that ZnO-NPs average crystallite size was 26.75 nm. These particle size values are in close agreement with those published by Ifeanyichukwu et al [35], who achieved "D" values of 28.41 nm. This outcome agreed with what the TEM analysis showed.

3.4. TEM Analysis.

The size and shape of the bio-formulated ZnO-NPs were studied using TEM examination[37]. Figure 5a shows the biogenic ZnO-NPs as spherical in shape. The spherical form of these nanoparticles sets them apart from other forms because of their large surface area and superior ability to penetrate bacterial structures. Spherically shaped nanoparticles are also beneficial

in biological applications [38]. Figure 5b shows the histogram pattern of biosynthesized ZnO-NPs varied in size from 10 to 72 nm in diameter, with an estimated average nano size of 25.75 nm. Based on the TEM results, the reactive bioactive elements in the aqueous medium support of the production of Zn-ONP using the aqueous extract of *A. ampeloprasum* leaves.

3.5. Energy dispersive X-ray scanning electron microscopy (EDX)

The existence of manufactured nanoparticles was further confirmed by SEM imaging and EDX analysis. Zinc oxide nanoparticles produced from the aqueous extract of *A. ampeloprasum* leaves have a rounded form and an agglomerated appearance, as seen in Figure 6a SEM image, similar to that described by Jayachandran et al [39]. The biologically produced ZnO-NPs were further analyzed using their EDX spectrum, shown in Figure 6b. The strong zinc metal peaks, containing oxygen, were confirmed by the EDX spectrum to be present in the *A. ampeloprasum* leaf aqueous extract-stabilized nanoparticles. The elemental analysis for ZnO-NPs shows that 26.06% of the components are oxygen and 58.31% are zinc. Furthermore, carbon peaks linked to biological constituents such as flavonoids, amino acids, polyphenols, vitamins, and saponins were observed.

3.6. Thermogravimetric (TGA) analysis.

The TGA performance of bio-fabricated ZnO-NPs is displayed in Figure 7. There were three significant weight loss periods identified. In First stage below 200 °C, there was a 15% weight loss due to the evaporation of water and the remaining living molecules on the organic surface moiety, which is hydrophilic. At 200 ◦C, the stabilizing capping agent *A. ampeloprasum* extract moieties continued to operate on the surface of the nanoparticles. The second stage, temperature increases between 200 and 440 °C were shown to cause a 20% drop in weight and to enhance the structural disruption of organic components [40]. ZnO-NPs stabilized by *A. ampeloprasum* extract resembled three different curves as temperatures increased; these curves were also previously seen in dextran-coated nanoparticles with magnetic characteristics [41].

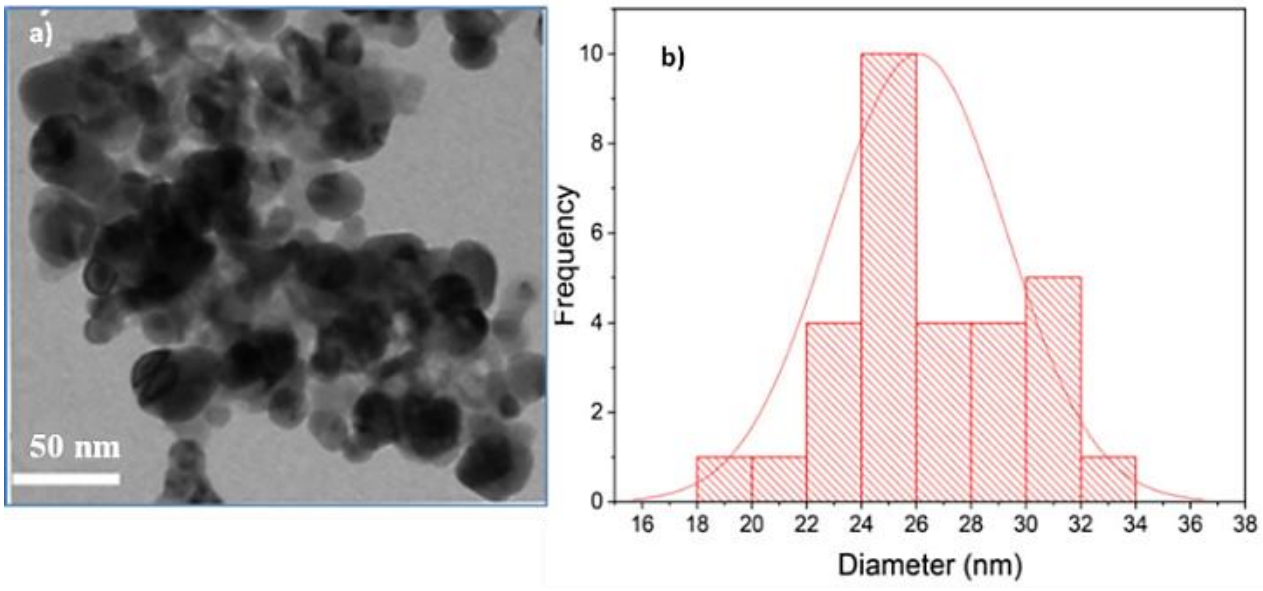

Figure. 5. (a) ZnO-NPs produced by extracting *A. ampeloprasum*, shown in TEM micrograph and (b) histogram of ZnO-NPs.

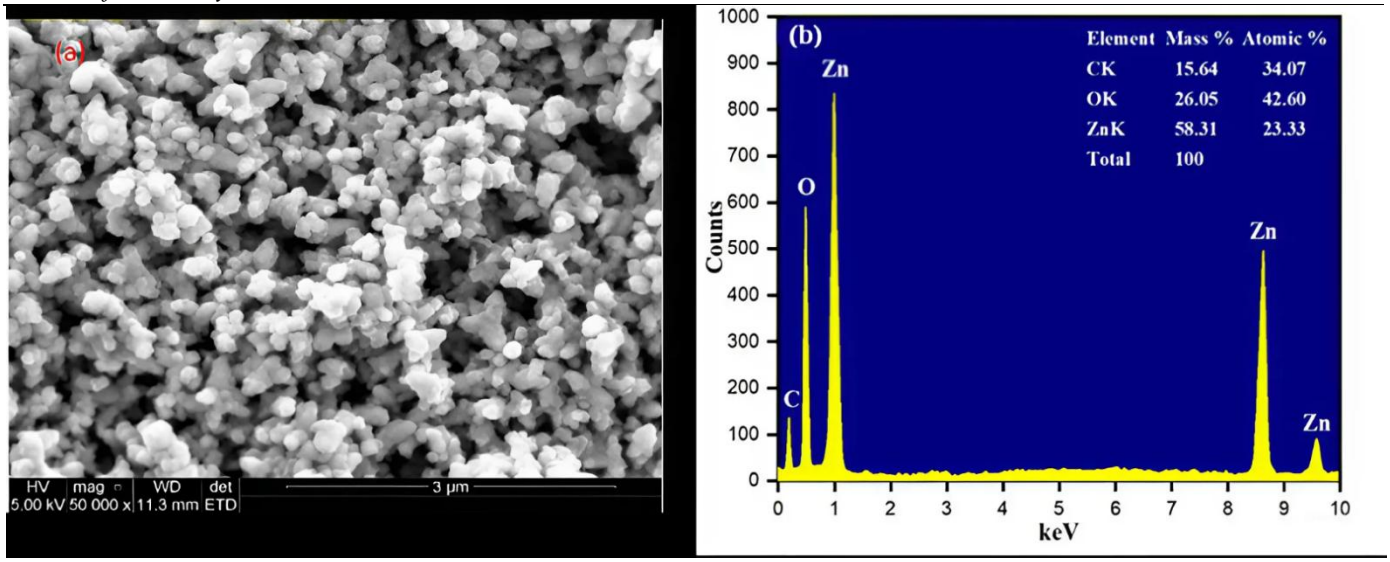

Figure 6. (a) The SEM picture displays EDX spectra of zinc oxide leaf aqueous extract from *A. ampeloprasum*. (b) The EDX spectrum of the aqueous extract *of A. ampeloprasum* leaves

The third stage resalts indicates that weight loss dropped by 10% at temperatures above 440–780°C, translating into a 55% weight reduction. Over 800°C, no appreciable weight loss was seen. The TGA results obtained for *A. ampeloprasum* extract highlight the possibility of organic chemicals acting as agents for capping nanoparticle surfaces and their ability to bio-generate ZnO-NPs.

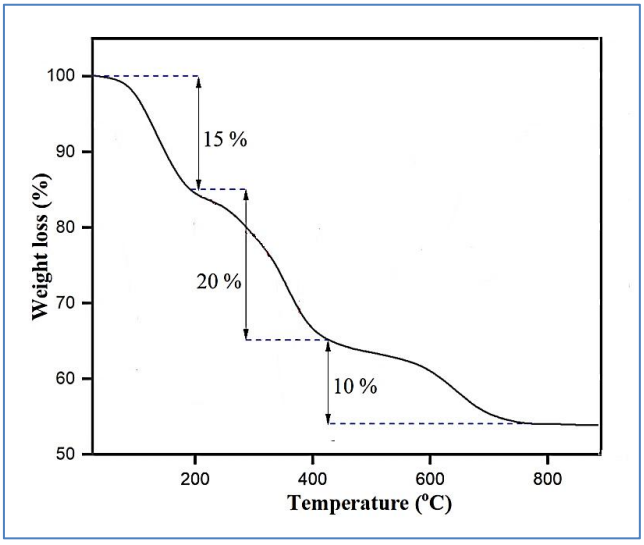

Figure 7. Bio-fabricated ZnO-NPs tested using TGA analysis.

3.7. The bio-fabricated ZnO-NPs' photocatalytic characteristics.

The bio-fabricated synthesized ZnO-NPs were tested for their efficiency for dye deterioration under UV light using methylene blue (MB) dye as a typical water contaminant. Several factors affect the nanoparticles' photocatalytic activity, such as size, surface area, pH, and sources of radiation. Stabilized ZnO-NPs derived from *A. ampeloprasum* extract were utilized for the MB dye's photocatalytic disintegration when exposed to a broad spectrum of UV light emitted by an Xe lamp (λ = 400 nm) at room temperature. Photocatalytic degradation by ZnO-NPs against MB is demonstrated in Figure 8a. The ideal absorption peak of MB, which was measured at 665 nm, was selected to examine the absorption throughout various time periods. The bio-fabricated ZnO-NPs had strong catalytic capabilities, as seen by the reduction of the absorbance peak at 665 nm within 120 minutes [9]. Different values of the degradation percentage were calculated over different periods of time. The biosynthesized ZnO-NPs degraded the MB dye by 90.13% after 120 minutes of UV exposure, as Figure 8b shows. The photodegradation efficiency of the dye MB is illustrated in Figure 9a. A 5-ppm dye solution was added to 50 mL of room temperature, pH 6 solution, varying the amounts of ZnO-NPs (5, 10, 15, 20, 25, and 40 mg). The findings proved that up to 20 mg of ZnO-NPs may be photodegraded more efficiently in *A. ampeloprasum* extract. An increase in the amount of catalytic activity means that there are more accessible active sites on the surface of catalyst [42]. However, photodegradation efficiency

dropped when the catalyst dosage was increased to more beyond 20 mg because to NP buildup and sedimentation. Because of the turbid and opaque suspension brought on by NP sedimentation, there was less light scattering and a higher catalytic load of NPs across the reaction mixture, which led to poor degradation [43]. Additionally, figure 9b contrasts the effects of higher dye concentrations (5, 10, and 15 ppm), room temperature, and UV light with the effects of ZnO-NP dosage (20 mg) at pH 6 on MB's photocatalytic degradation. Interestingly, ZnO-NPs in the extract of *A. ampeloprasum* showed better photodegradation efficiency at the lowest dye concentration of 5 ppm. The effectiveness of photocatalytic degradation mediated by NPs decreased when the dye concentration was initially increased from 5 to 15 ppm, indicating that the MB dye concentration was required for this activity. But it's important to keep in mind that compared to the reaction mixture including ZnO-NPs, the catalyst is more effective in generating •OH and O_2• at 15 ppm MB, which speeds up the photodegradation of MB [44]. As seen in Figure 9c, changing the pH from 2 to 10 and the room temperature influenced the ZnO-NPs in the *A. ampeloprasum* leaf extract for MB's photocatalytic degradation at fixed dye levels of 5 ppm and catalyst concentrations of 20 mg. Alkaline environments at pH 8 and 10 showed the highest percentage of MB degradation.

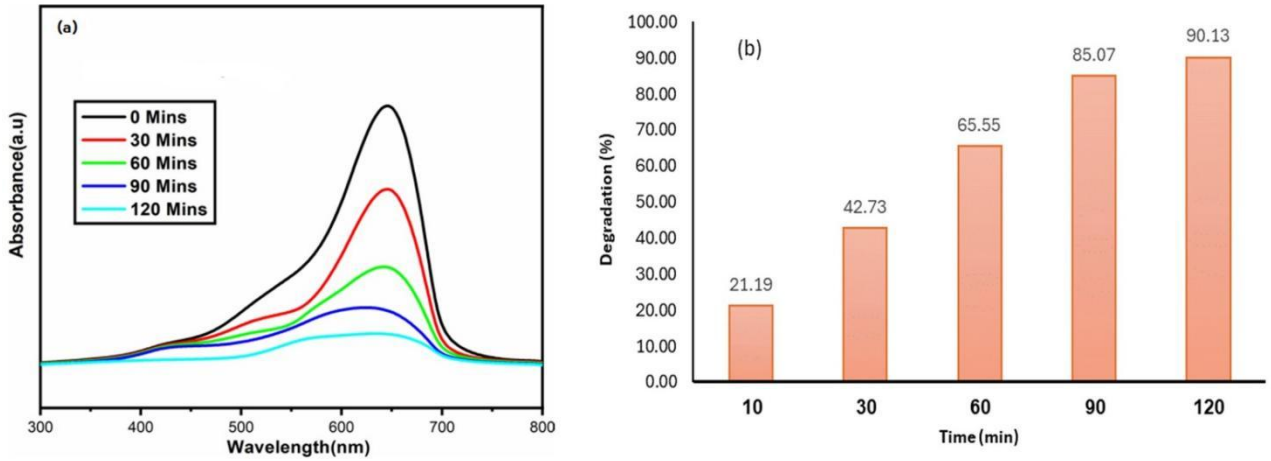

Figure 8. (a) A typical absorbance spectrum of MB dye under UV light with bio-fabricated ZnO-NPs present. (b) The percentage of MO dye degradation at various periods.

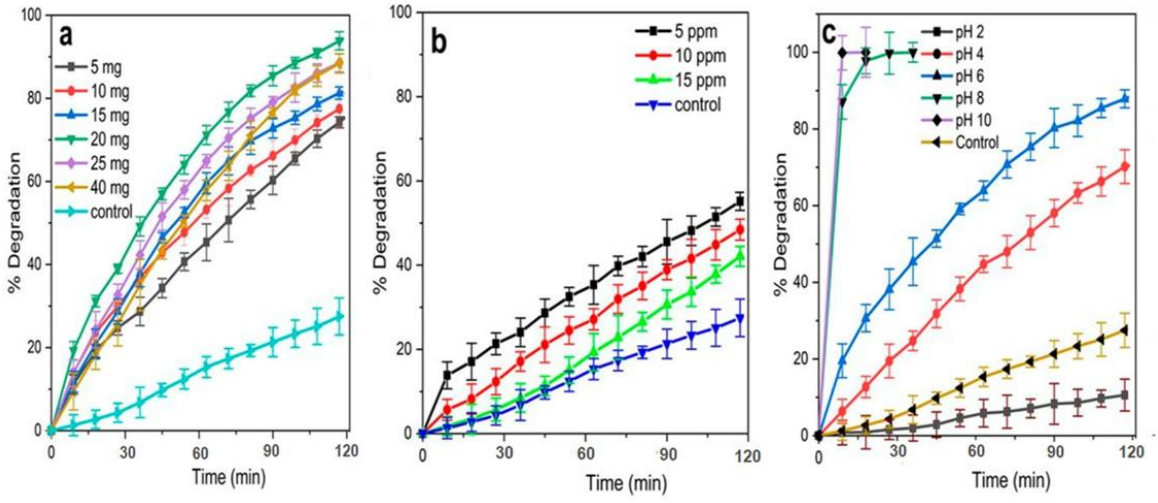

Figure 9. Parameters of physico-chemical optimization for photocatalytic degradation with ZnO-NPs in A. ampeloprasum leaf extract are presented. (a) ZnO-NPs catalytic load; (b) MB concentration with a constant catalytic load of 20 mg (c) pH at a constant dye concentration of 5 ppm and a catalytic load of 20 mg.

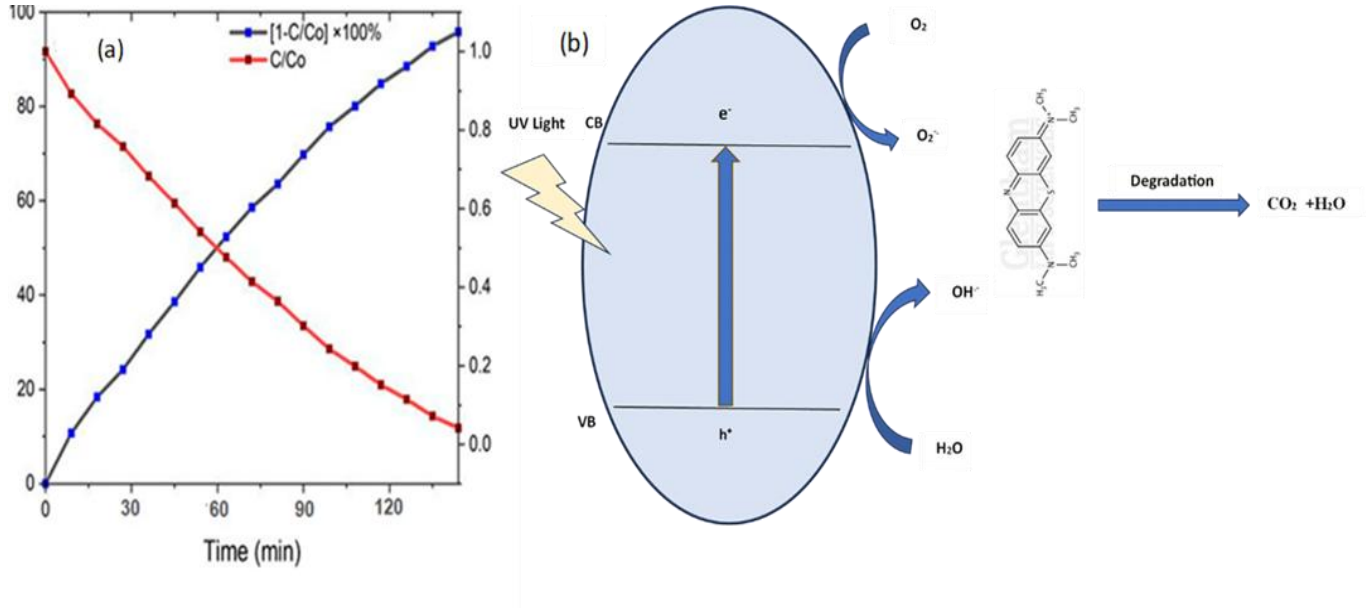

Figure 10. (a) ZnO-NPs photocatalytic degradation plots for MB dye generated with half-lives of A. ampeloprasum leaf extract. (b) Shows the potential process for the photocatalytic degradation of MB dye.

However, ZnO-NPs lessen the effectiveness of their photocatalytic destruction of MB since they break down more readily in acidic settings (pH 2 and 4). The literature suggests that zero potential charges might be used to explain this [45]. The pH medium selected for the MB dye degradation experiment was pH 6, as it is challenging to observe the reaction at pH 8 or 10. The dye bonding was lessened by surface electron migration. When nanoparticles are present during excitation, their active sites are significantly higher than in nanoparticle samples that are not exposed to light [46]. In the process of photocatalysis, conduction band electrons on the photocatalyst material were induced to move from the valence band. Additionally, the valence band had an equal number of holes in it. Subsequently, the trapped electrons and conduction-band electrons traveled jointly to the photocatalyst's surface, where the oxygen vacancies had imprisoned them [47]. Superoxide radicals (O_2−•) were created because of the oxygen vacancies trapping the O_2 molecules. Meanwhile, the oxygen molecules are in MB dye solution are converted into superoxide radicals by interacting with oxygen vacancies on the surface [48]. Hydrogen (H_2O) molecules or OH− groups also captured holes, resulting in the production of hydroxyl radicals ($OH^{\bullet-}$). The target dye is eventually successfully degraded by the produced radicals' interactions with the contaminant. In the presence of biosynthesized ZnO-NPs, MB photocatalytic degradation is schematically represented in Figure 10b, with corresponding equations displayed in (4 to 9) [48].

$$ZnO + h\nu \rightarrow e^- + h^+ \quad (4)$$

$$O_2 + e^- \rightarrow O_2^{-\bullet} \quad (5)$$

$$h^+ + OH^- \rightarrow OH. \quad (6)$$

$$h^+ + H_2O \rightarrow H^+ + OH.- \quad (7)$$

$$MB + OH.^- \rightarrow CO_2 + H_2O \quad (8)$$

$$MB + \dot{O_2^-} \rightarrow CO_2 + H_2O \quad (9)$$

3.8. Antimicrobial efficacy

The antimicrobial efficacy of the NPs was examined using the disc diffusion technique against the bacteria *E. coli* and *S. aureus*, both gram-positive and gram-negative. The antibacterial nanoparticles' inhibiting zone is shown in Figure 11(a). ZnO-

NPs linked to plant extracts showed the strongest inhibition at different doses. Green-assisted ZnO-NPs have far better bacterial sensitivity against *S. aureus* than against *E. coli*. Figure 11(b) illustrates the disk with green-synthesized ZnO-NPs at various concentrations and their corresponding inhibitory zones (mm). Synthesized ZnO-NPs were more effective at a concentration of 100 µg/mL than at a lower concentration of 10 µg/mL. These results are consistent with the results of previous studies [5]. According to Table 1, the synthesized ZnO-NPs demonstrated the highest zone inhibition (15.01 ± 0.85 mm) for *S. aureus* versus *E. coli* (13.34 ± 0.04 mm). The production of Zn^{+2} ions control the growth and spread of E. Coli and Aureus bacteria.

Table 1. The average inhibitory zones value (mm) was obtained from the *A. ampeloprasum* leaf extract mediated by zinc oxide nanoparticles.

N	Bacterial strains	10µg/ml (mm)	20µg/ml (mm)	50µg/ml (mm)	100µg/ml (mm)
1	S. aureus	7.16 ± 0.76	12.33 ± 0. 49	12.93 ± 0.45	15.01 ± 0.85
2	E. coli	8.14 ± 0.52	10.10 ± 1.00	12.20 ± 0.07	13.34 ± 0.04

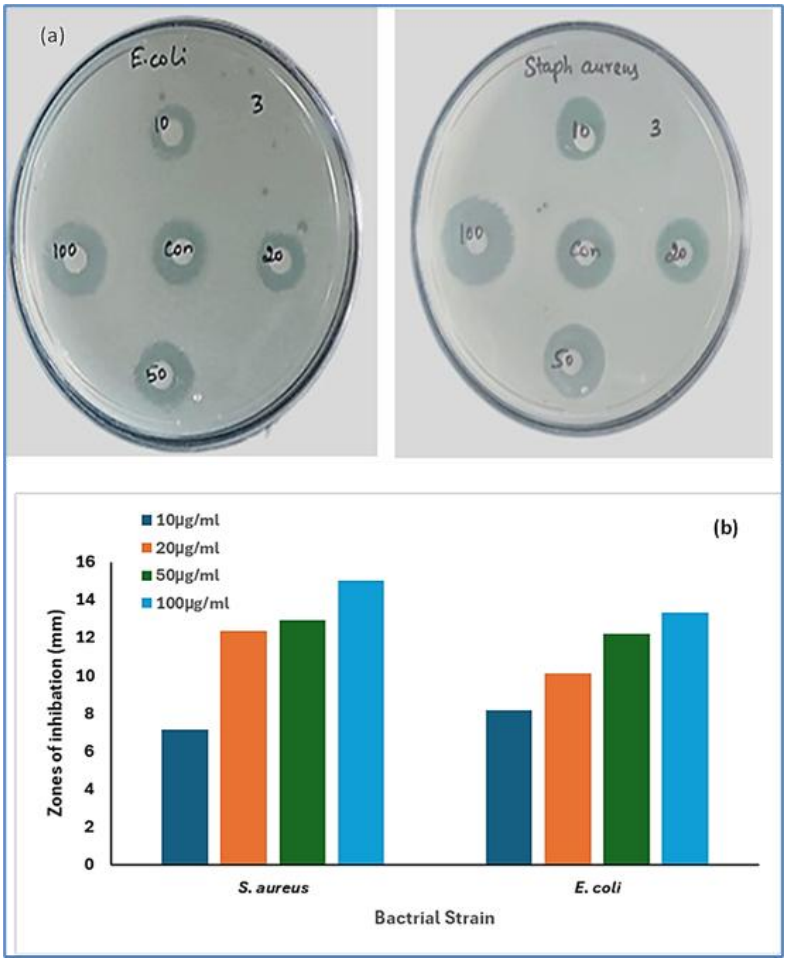

Figure 11. (a) ZnO-NPs that have been biosynthesized demonstrate efficacious antibacterial properties against both E. Coli and S. aureus (b) The antibacterial activity of ZnO-NPs was investigated in bar graphs at four distinct concentrations (10 µg/mL, 20 µg/mL, 50 µg/mL, and 100 µg/mL), which were mediated by *A. ampeloprasum* leaf extract.

The release of Zn^{+2} ions resulted in leaks in the cell wall membrane and, consequently suppression of the bacteria. The amikacin antibiotic disc increases the obtained values of bacterial inhibition. The use of plant extracts with zinc oxide nanoparticles (ZnO-NPs) enhances the production of free radicals and increases oxidative activity [42]. The bacterial structure allowed metal ions to enhance electrostatic contact and cause ZnO-NPs to produce ROS [49]. Furthermore, DNA and protein molecules' deactivation state is the source of metal ion and lattice oxygen dissolution. The bacterial system's damage to its DNA and proteins cuts off its feeding and communication systems, which results in cell death [50].

4. Conclusion

In this work, an aqueous extract of *A. ampeloprasum (leek)* leaves is used to produce ZnO-NPs based on phytochemicals. Several microscopic and spectroscopic methods were used to assess the structural characteristics of the bio-fabricated ZnO-NPs. The ZnO-NPs that were bio-fabricated exhibited a band gap of 2.95 eV and an average particle size of 25.75 nm. The bio-fabricated ZnO-NPs effectively functioned as photocatalysts degrading MB (methyl blue) dye at a rate of 90.13% when exposed to UV light. When it came to S. aureus, the bacterially deactivated ZnO-NPs outperformed E. coli in terms of inhibition. The findings suggest that ZnO-NPs might be a good choice for wastewater treatment, pathogen inactivation agents, and hazardous dye photoelimination.

Authors Contribution

Nabil A. Alhemiary Conceptualization, methodology, preparation of nanocomposite and writing original draft preparation. Yasser. S. Ibrahem formal analysis, antibacterial activity, review.

Conflicts of Interest

There are no conflicts of interest reported by the writers.

Data Availability statement

The data presented in this study are available on request from the corresponding author.

Funding

The author(s) received no financial support fortheresearch, authorship, and/or publication of this article.

REFERENCES

1. Shahzad K, Hussain S, Altaf Nazir M, Jamshaid M, ur Rehman A, Alkorbi AS, et al. Versatile Ag2O and ZnO nanomaterials fabricated via annealed Ag-PMOS and ZnO-PMOS: An efficient photocatalysis tool for azo dyes. J Mol Liq. 2022;356:119036. https://doi.org/10.1016/j.molliq.2022.119036
2. Malik AR, Sharif S, Shaheen F, Khalid M, Iqbal Y, Faisal A, et al. Green synthesis of RGO-ZnO mediated Ocimum basilicum leaves extract nanocomposite for antioxidant, antibacterial, antidiabetic and photocatalytic activity. J Saudi Chem Soc. 2022;26(2):101438. https://doi.org/10.1016/j.jscs.2022.101438
3. Denisa-Maria R, Vasile-Adrian S, Anton F, Denisa F, Alexandru-Mihai G, Ecaterina A. Green Synthesis of Metal and Metal Oxide Nanoparticles: A Review of the Principles and Biomedical Applications. Int J Mol Sci. 2023; 24(20): 15397. https://doi.org/10.3390/ijms242015397
4. Singh J, Dutta T, Kim KH, Rawat M, Samddar P, Kumar P. "Green" synthesis of metals and their oxide nanoparticles: Applications for environmental remediation. J Nanobiotechnology. 2018;16(1):1–24. https://doi.org/10.1186/s12951-018-0408-4
5. Wu H, Shen W, Zhao Q, Zhang W. Synthesis of chitosan-based flocculant by dielectric barrier discharge modification and its flocculation performance in wastewater treatment. RSC Adv. 2024;14(4):2410–21. https://doi.org/10.1039/d3ra06265a.
6. Premanathan M, Karthikeyan K, Jeyasubramanian K, Manivannan G. Selective toxicity of ZnO nanoparticles toward Gram-positive bacteria and cancer cells by apoptosis through lipid peroxidation. Nanomedicine

Nanotechnology, Biol Med. 2011;7(2):184–92. https://doi.org/10.1016/j.nano.2010.10.001

7. Gonçalves RA, Toledo RP, Joshi N, Berengue OM. Green synthesis and applications of ZnO and TiO2 nanostructures. Molecules. 2021;26(8). https://doi.org/10.3390/molecules26082236
8. Von White G, Kerscher P, Brown RM, Morella JD, McAllister W, Dean D, et al. Green synthesis of robust, biocompatible silver nanoparticles using garlic extract. J Nanomater. 2012;2012:55. https://doi.org/10.1155/2012/730746
9. Pal S, Pal K, Mukherjee S, Bera D, Karmakar P, Sukhen D. Green cardamom mediated phytosynthesis of ZnONPs and validation of its antibacterial and anticancerous potential. Mater Res Express. 2020;7(1):15068. https://doi.org/ 10.1088/2053-1591/ab69c8
10. Abel S, Tesfaye JL, Shanmugam R, Dwarampudi LP, Lamessa G, Nagaprasad N, et al. Green synthesis and characterizations of zinc oxide (ZnO) nanoparticles using aqueous leaf extracts of coffee (Coffea arabica) and its application in environmental toxicity reduction. J Nanomater. 2021;2021:1–6. https://doi.org/10.1155/2021/3413350
11. Kebede Urge S, Tiruneh Dibaba S, Belay Gemta A. Green Synthesis Method of ZnO Nanoparticles using Extracts of Zingiber officinale and Garlic Bulb (Allium sativum) and Their Synergetic Effect for Antibacterial Activities. J Nanomater. 2023;2023. https://doi.org/10.1155/2023/7036247
12. Doan Thi TU, Nguyen TT, Thi YD, Ta Thi KH, Phan BT, Pham KN. Green synthesis of ZnO nanoparticles using orange fruit peel extract for antibacterial activities. RSC Adv. 2020. 10: 23899–23907. https://dio.org/10.1039/D0RA04926C
13. Demissie MG, Sabir FK, Edossa GD, Gonfa BA. Synthesis of zinc oxide nanoparticles using leaf extract of lippia adoensis (koseret) and evaluation of its antibacterial activity. J Chem. 2020;2020:1–9. https://doi.org/10.1155/2020/7459042
14. Shahrajabian MH, Sun W, Cheng Q. A Review of Leek (A. ampeloprasum L.), an Important Vegetable and Food Ingredient with Remarkable Pharmaceutical Activities. Pharmacogn Commun. 2021;11(1):9–12. https://doi.org/10.5530/pc.2021.1.3
15. Abbas MA. Analgesic effect of Allium ampeloprasum: Evidence for the involvement of beta-adrenergic system. J Funct Foods. 2019;57:1–6. https://doi.org/10.1016/j.jff.2019.03.046
16. Adão CR, da Silva BP, Parente JP. A new steroidal saponin with antiinflammatory and antiulcerogenic properties from the bulbs of Allium ampeloprasum var. porrum. Fitoterapia. 2011;82(8):1175–80. h https://doi.org/10.1016/j.fitote.2011.08.003
17. Najda A, Błaszczyk L, Winiarczyk K, Dyduch J, Tchórzewska D. Comparative studies of nutritional and health-enhancing properties in the "garlic-like" plant Allium ampeloprasum var. ampeloprasum (GHG-L) and A. sativum. Sci Hortic (Amsterdam). 2016;201:247–55. https://doi.org/10.1016/j.scienta.2016.01.044
18. Emir C, Coban G, Emir A. Metabolomics profiling, biological activities, and molecular docking studies of elephant garlic (Allium ampeloprasum L.). Process Biochem. 2022;116:49–59. https://doi.org/10.1016/j.procbio.2022.03.002
19. Bareemizadeh F, Ghasempour H, Maassoumi SM, Karimi N, Taran M, Ghasempour M. In vitro antimicrobial activity of Allium ampeloprasum L. var. atroviolaceum Regel. Int J Biosci. 2014;4(5):80–4. http://dx.doi.org/10.12692/ijb/4.5.80-84
20. Nallal VUM, Padmini R, Ravindran B, Chang SW, Radhakrishnan R, Almoallim HSM, et al. Combined in vitro and in silico approach to evaluate the inhibitory potential of an underutilized allium vegetable and its pharmacologically active compounds on multidrug resistant Candida species. Saudi J Biol Sci. 2021;28(2):1246–56.

https://doi.org/10.1016/j.sjbs.2020.11.082

21. Rasool S, Al Meslmani B, Alajlani M. Determination of Hypoglycemic, Hypolipidemic and Nephroprotective Effects of Berberis Calliobotrys in Alloxan-Induced Diabetic Rats. Molecules. 2023;28(8). https://dio.org/10.3390/molecules28083533
22. Uma Maheshwari Nallal V, Prabha K, VethaPotheher I, Ravindran B, Baazeem A, Chang SW, et al. Sunlight-driven rapid and facile synthesis of Silver nanoparticles using Allium ampeloprasum extract with enhanced antioxidant and antifungal activity. Saudi J Biol Sci. 2021;28(7):3660–8. https://doi.org/10.1016/j.sjbs.2021.05.001
23. Shaheen S, Iqbal A, Ikram M, Imran M, Naz S, Ul-Hamid A, et al. Graphene oxide-ZnO nanorods for efficient dye degradation, antibacterial and in-silico analysis. Appl Nanosci. 2022;1–13. https://doi.org/10.1007/s13204-021-02251-2
24. Bale VK, Katreddi HR. Synthesis, characterization and catalytic activity of zinc oxide nanoparticles functionalized with metallo-thoiosemicarbazones. Asian J Nanosci Mater. 2022;5(2):159–73. https://doi.org/10.26655/AJNANOMAT.2022.2.7
25. Steffy T, Gayathiri G, Vijaya A A, Saradhadevi M. Synthesis and Characterization of Zinc Oxide Nanoparticles of Solanum nigrum and Its Anticancer Activity via the Induction of Apoptosis in Cervical Cancer. Biol Trace Elem Res. 2022; 200(6):2684-2697. https://doi.org/ 10.1007/s12011-021-02898-6
26. Ahmed A, Usman M, Yu B, Ding X, Peng Q, Shen Y, et al. Efficient photocatalytic degradation of toxic Alizarin yellow R dye from industrial wastewater using biosynthesized Fe nanoparticle and study of factors affecting the degradation rate. J Photochem Photobiol B Biol. 2020;202:111682. https://doi.org/10.1016/j.jphotobiol.2019.111682
27. Ananda A, Ramakrishnappa T, Ravishankar T N, Archana S, Shilpa B M, Reddy yadav L S, Jayanna B K. Optimization and Numerical investigation of organic dye degradation using Response Surface by green synthesized ZrO2 nanoparticles and its antibacterial activity. 2022;7(3) 267-287. https://doi.org/10.22090/jwent.2022.03.004
28. Jubu PR, Chahrour KM, Muhammad A, Lamido S, Kan-Hausa U, Landi S, et al. Considerations About the Determination of Optical Bandgap from Diffuse Reectance Spectroscopy Using the Tauc Plot. 2023;1–19. https://doi.org/10.21203/rs.3.rs-2654236/v1
29. Musleh H, Zayed H, Shaat S, Tamous HM, Asad J, Al-Kahlout A, et al. Synthesis and characterization of ZnO nanoparticles using sol gel technique for dye sensitized solar cells applications. J Phys Conf Ser. 2019;1294(2). https://doi.org/10.1088/1742-6596/1294/2/022022
30. Ibrahim N A, Seham S. E, Zeinab A. K, Zeinab A, Kandil S, Essam M A ,Yasmine S M ,Abdulrahman MS, Mohamed A. Green Synthesized Zinc Oxide Nanoparticles Based on Cestrum diurnum L. of Potential Antiviral Activity against Human Corona 229-E Virus. Molecules 2023, 28(1), 266. https://doi.org/10.3390/molecules28010266
31. Ansari AA, Abushad M, Arshad M. Swaleha N, Hilal A, Shahid H, Wasi K. Microstructure, Optical and Dielectric Properties of Cobalt-doped Zinc ferrite Nanostructures. J Mater Sci: Mater Electron. 2021; 32; 21988–22002. https://doi.org/10.1007/s10854-021-06647-2
32. Abdulmalek S, Eldala A, Awad D, Balbaa M. Ameliorative effect of curcumin and zinc oxide nanoparticles on multiple mechanisms in obese rats with induced type 2 diabetes. Sci Rep. 2021;11(1):1–22. https://doi.org/10.1038/s41598-021-00108-w
33. Khan MS, Dhavan PP, Jadhav BL, Shimpi NG. Ultrasound-Assisted Green Synthesis of Ag-Decorated ZnO Nanoparticles UsingExcoecaria agallochaLeaf Extract and Evaluation of Their Photocatalytic and Biological Activity. ChemistrySelect. 2020;5(41):12660–71. https://doi.org/10.1002/slct.202002905

34. Al-Khaial MQ, , Siok Yee Chan , Rund A. Abu-Zurayk NA. Biosynthesis and Characterization of Zinc Oxide Nanoparticles (ZnO-NPs) Utilizing Banana Peel Extract. inorganics. 2024;12(121):1–25. https://doi.org/10.3390/inorganics12040121
35. Narges C, Nabi J, Niloofar N. Rapid biosynthesis and antibacterial activity of zinc oxide nanoparticles using fruit peel of Punica granatum L as cellulose. Current Research in Green and Sustainable Chemistry. 2023; 6; 100366. https://doi.org/10.1016/j.crgsc.2023.100366
36. Sahu S, Samanta PK. Peak Profile Analysis of X-ray Diffraction Pattern of Zinc Oxide Nanostructure. J Nano- Electron Phys. 2021;13(5):1–4. https://dio.org/10.21272/jnep.13(5).05001
37. Ngoepe NM, Mbita Z, Mathipa M, Mketo N, Ntsendwana B, Hintsho-Mbita NC. Biogenic synthesis of ZnO nanoparticles using Monsonia burkeana for use in photocatalytic, antibacterial and anticancer applications. Ceram Int. 2018;44(14):16999–7006. https://doi.org/10.1016/j.ceramint.2018.06.142
38. Pandit C, Roy A, Ghotekar S, Khusro A, Islam MN, Emran T Bin, et al. Biological agents for synthesis of nanoparticles and their applications. J King Saud Univ - Sci. 2022;34(3):101869. https://doi.org/10.1016/j.jksus.2022.101869
39. Jayachandran A, T.R. A, Nair AS. Green synthesis and characterization of zinc oxide nanoparticles using Cayratia pedata leaf extract. Biochem Biophys Reports. 2021;26:100995. https://doi.org/https://doi.org/10.1016/j.bbrep.2021.100995.
40. Chen WH, Lin BJ, Lin YY, Chu YS, Ubando AT, Show PL, et al. Progress in biomass torrefaction: Principles, applications and challenges. Prog Energy Combust Sci. 2021;82:100887. https://doi.org/10.1016/j.pecs.2020.100887.
41. Faridul M I, Anik K S, Shariful I , Miah MAS , Mou JT, Obidul AK Huq, Mondol Md H. Bhuiyan M N I. Green synthesis of zinc oxide nano particles using Allium cepa L. waste peel extracts and its antioxidant and antibacterial activities. Heliyon, Volume 10, Issue 3, e25430. https://doi.org/10.1016/j.heliyon.2024.e25430
42. Eskandarinezhad S, Khosravi R, Amarzadeh M, Mondal P, Magalhães Filho F J C. Application of different Nanocatalysts in industrial effluent treatment: A review. Journal of Composites and Compounds. 2021; 3(6): 43–56. https://doi.org/10.52547/jcc.3.1.5
43. Tegenaw AB, Yimer AA, Beyene TT. Boosting the photocatalytic activity of ZnO-NPs through the incorporation of C-dot and preparation of nanocomposite materials. Heliyon. 2023;9(10):e20717. https://doi.org/10.1016/j.heliyon.2023.e20717
44. Chiu YH, Chang TFM, Chen CY, Sone M, Hsu YJ. Mechanistic insights into photodegradation of organic dyes using heterostructure photocatalysts. Catalysts. 2019;9(5). https://doi.org/10.3390/catal9050430
45. Kumar MRA, Ravikumar CR, Nagaswarupa HP, Purshotam B, Gonfa B, Murthy HCA, et al. Evaluation of bi-functional applications of ZnO nanoparticles prepared by green and chemical methods. J Environ Chem Eng. 2019;7(6):103468. https://doi.org/https://doi.org/10.1016/j.jece.2019.103468.
46. R Usman Q, Jahan Z H, Rukhsar A B. Raza A, Ghazanfar N, Walid N, Kram M. Photocatalysis vs adsorption by metal oxide nanoparticles, J Mater Sci & Techn. 2022;131(21): 122-166. https://doi.org/10.1016/j.jmst.2022.05.020
47. Ragupathy S, Manikandan V, Devanesan S, Ahmed M, Ramamoorthy M, Priyadharsan A. Enhanced sun light driven photocatalytic activity of Co doped SnO2 loaded corn cob activated carbon for methylene blue dye degradation.. Chemosphere. 2022, 295:133848. https://doi.org/10.1016/j.chemosphere.2022.133848
48. Alkorbi AS, Muhammad Asif Javed H, Hussain S, Latif S, Mahr MS, Mustafa MS, et al. Solar light-driven photocatalytic degradation of methyl blue by carbon-doped TiO2 nanoparticles. Opt Mater (Amst).

2022;127(March):112259. https://doi.org/10.1016/j.optmat.2022.112259

49. Sirelkhatim A, Mahmud S, Seeni A, Kaus NHM, Ann LC, Bakhori SKM, et al. Recent Advances in Zinc Oxide Nanostructures with Antimicrobial Activities. Int. J. Mol. Sci. 2020, 21(22), 8836; https://doi.org/10.3390/ijms21228836
50. Yuchao Li,Chengzhu L, Sie C T . Zinc oxide nanoparticles prepared through microbial mediated synthesis for therapeutic applications: a possible alternative for plants. Front Microbiol. 2023;14(September):1–20. https://doi.org/10.3389/fmicb.2023.1227951.

How to cite this article:
Alhemiary NA, Ibrahem YS. (2024). Biosynthesis, characterization, antibacterial activities, and photocatalysis of zinc oxide nanoparticles using Allium ampeloprasum (leeks) leaves extract. Journal of Chemistry and Environment. 3(2). p. 1-15.